Journal of South American Earth Sciences 28 (2009) 217–228

Contents lists available at ScienceDirect

Journal of South American Earth Sciences

journal homepage: www.elsevier.com/locate/jsames

Characterization of Quaternary faults by electric resistivity tomography in the Andean Precordillera of Western Argentina

Sabrina Y. Fazzito [a,*], Augusto E. Rapalini [a], José M. Cortés [b], Carla M. Terrizzano [b]

[a] Consejo Nacional de Investigaciones Científicas y Técnicas (CONICET), Instituto de Geofísica Daniel Valencio (INGEODAV), Departamento de Ciencias Geológicas, Facultad de Ciencias Exactas y Naturales, Universidad de Buenos Aires, Pabellón II, Ciudad Universitaria, C1428EHA, Buenos Aires, Argentina
[b] Consejo Nacional de Investigaciones Científicas y Técnicas (CONICET), Laboratorio de Neotectónica (LANEO), Departamento de Ciencias Geológicas, Facultad de Ciencias Exactas y Naturales, Universidad de Buenos Aires, Pabellón II, Ciudad Universitaria, C1428EHA, Buenos Aires, Argentina

ARTICLE INFO

Article history:
Received 10 April 2008
Accepted 1 June 2009

Keywords:
Electrical Resistivity Tomography
Geoelectrical method
Quaternary faults
Neotectonics
Precordillera
Andes
Argentina

ABSTRACT

Structural and geomorphic surface observations are frequently insufficient for a proper geometric and kinematic characterization of Quaternary faults. In order to improve the geological knowledge of three Quaternary faults in the Precordillera of western Argentina (30°46′ S–32°24′ S, 69°07′ W–69°15′ W), a shallow 2D Electrical Resistivity Tomography (ERT) survey was performed along seven short cross-sections, perpendicular to the fault traces. The survey was carried out across the San Bartolo fault, the Los Avestruces high and the El Tigre fault in the Precordillera of western Argentina in the San Juan and Mendoza provinces. During the survey, different electrical arrangements were assessed, including different arrays (dipole–dipole and Wenner–Schlumberger), diverse electrode separations and different depth of investigation. Tomographic models showed low resistivity zones lying below the fault scarps, as well as significant resistivity contrasts across the inferred fault-zones in the subsurface. This information permitted better characterization of the geometry and kinematics of these fault zones. ERT results showed that the San Bartolo fault is extensional. In the Los Avestruces high a positive inversion of an extensional fault was recorded by the electrical images. In the resistivity sections of the El Tigre strike-slip fault, a near vertical fault plane associated with blind splays could be identified. Our results confirm that the resistivity method is a valuable tool to image fault planes and to characterize the general geometry of extensional, reverse and strike slip faults at depth.

1. Introduction

Stratigraphic, structural and geomorphic studies are the usual methods that have been employed in the recognition and characterization of Quaternary faults in Argentina. Investigation of Quaternary tectonic activity has generally relied on superficial evidence of Quaternary deformation and the subsequent determination of the geometry and kinematics of the involved structures. Geomorphic features, like piedmont or bedrock scarps, pressure ridges and sag ponds are the main evidence of Quaternary faulting in the Precordillera of western Argentina (Bastías et al., 1990, 1993; Cortés et al., 1999b; Costa et al., 2000b). Although the trace of the fault plane is sometimes easily recognized in the field, the subsurface structural configuration is inferred only from the surficial features and trench data. These, however, are often poorly preserved or have an incomplete expression. Due to the limited depth of exposure, trench logging information does not necessarily represent the geometry of major faults at depth. Fortunately, in many cases, different geophysical techniques, such as shallow to standard reflection seismology, ground penetrating radar or potential methods as gravity or magnetics, have proved to be successful in determining the geometry and some structural features of the fault zone in the first tens to several hundred meters below surface (e.g. Wang, 2002; Donne et al., 2007). A relatively recent geophysical method applied to this objective is the electric resistivity tomography (ERT, e.g.: Fleta et al., 2000; Giano et al., 2000; Storz et al., 2000; Suzuki et al., 2000; Verbeeck et al., 2000; Demanet et al., 2001a, 2001b; Caputo et al., 2003, 2007; Wise et al., 2003; Colella et al., 2004; Rizzo et al., 2004; Nguyen et al., 2005, 2007). By imaging the fault zone to depths up to around 100 m, this geophysical technique, together with geological studies and ages of deformation, can help in achieving a better definition of the neotectonic activity of an area. Among the main specific targets of the geoelectrical investigation of fault zones, are the geometry of the fault plane, the presence, number and distribution of associated splays and blind faults, and the throw estimation. In spite of several successful cases, the geoelectrical investigation of fault zones has not yet been globally adopted as a customary technique in studies of Quaternary tectonics or seismic hazard assessments.

* Corresponding author. Tel./fax: +54 11 4788 3439.
E-mail addresses: sabrinafazzito@gl.fcen.uba.ar (S.Y. Fazzito), rapalini@gl.fcen.uba.ar (A.E. Rapalini), cortes@gl.fcen.uba.ar (J.M. Cortés), cterrizzano@gl.fcen.uba.ar (C.M. Terrizzano).

0895-9811/$ - see front matter © 2009 Elsevier Ltd. All rights reserved.
doi:10.1016/j.jsames.2009.06.001

In this contribution we present the results of 2D ERT across three Quaternary fault systems in the Precordillera of the Central Andes of western Argentina. Our aims have been to further investigate the capabilities and limitations of this technique when applied to fault zones and to better constrain the geometry and tectonic regime of these three areas. Quaternary tectonic evolution of the Precordillera of Mendoza and San Juan, in western Argentina, has been reviewed by Cortés and Costa (1996), Cortés et al. (1999b, 2006), Costa et al. (1999, 2000a,b, 2006) and Siame et al. (2006), providing contributions towards a better understanding of the seismic hazard of the region. However, and in spite of their well known advantages, shallow geophysical methods have not been used yet in this region to investigate tectonically active areas. The results of 10 ERT along seven profiles performed across three Quaternary fault zones in the Precordillera of western Argentina are analyzed and interpreted within the geological context. The studied faults are the regional San Bartolo fault, with poor kinematic evidence at surface, the regional strike-slip El Tigre fault and a minor reverse fault at the Los Avestruces high. These partially different tectonic settings provided further possibilities to get insights into the capabilities and limitations of the ERT technique.

2. Neotectonics of the Precordillera

The Precordillera of western Argentina is a first order morphotectonic unit uplifted during the Late Cenozoic on the southern flat-slab segment (28° S–33° S) of the Central Andes. Its Neogene tectonic evolution results from the migration towards the east of the magmatic arc and the contractional and transpressive deformation of the foreland basin as a consequence of gradual flattening of the Nazca plate in the last 20 Myr (Isacks and Barazangi, 1977; Jordan et al., 1983).

The central segment of the Precordillera (Fig. 1), between 30° S and 31°30′ S in the San Juan province, is an east verging thin-skinned belt (Baldis et al., 1982; von Gosen, 1992). This thrusted and folded system exhibits in its eastern margin an opposite vergence with a deeper level of detachment in the basement, defining there a thick skinned triangle zone (Zapata and Allmendinger, 1996).

In contrast with the central segment, the Late Cenozoic tectonics of the southern section of the Precordillera, located mainly in the Mendoza province (31°30′–33° S, see Fig. 1), has evolved under the influence of structural anisotropies as oblique megashear zones and paleogeographic features of Paleozoic and Triassic age (Kozlowski et al., 1993; Cortés et al., 2005a; Cortés et al., 2006). Consequently, this morphotectonic unit, named the Precordillera Sur (Cortés et al., 2005b), shows a more complex structure, characterized by a combination of tectonic inversion of extensional Triassic half-grabens (Legarreta et al., 1993; Ramos and Kay 1991; Cortés et al., 1999a), the contractional and transpressive rejuvenation of Permian structures (von Gosen, 1995; Cortés et al., 1999a) and strike-slip displacements on NW trending faults (Cortés et al., 2005a).

The northern margin of the Precordillera Sur is defined by a Late Cenozoic deformation zone (the Barreal-Las Peñas belt), which is a left-lateral transpressive belt crossing the whole Precordillera from the Barreal region in the northwest to Sierra de Las Peñas in the southeast (Cortés et al., 2006). This tectonic feature consists of five left-stepping faulted blocks bounded by oblique strike-slip fault systems.

In the central section of the Precordillera (30°00′ S–31°30′ S), Quaternary ruptures generally result from the reverse and oblique rejuvenation along segments of range-front faults. Other evidence is commonly exposed at intermontane basins as fault scarps developed in alluvial fans of piedmont areas (Bastías et al., 1990; Cortés et al., 1999b; Costa et al., 2000b). The eastern flank of the Precordillera, between 31° and 34° S concentrates most of this Quaternary and active deformation (Costa et al., 2006). Nevertheless, as a consequence of strain partitioning, Pleistocene sediments at the western flank have been displaced along the 120-km-long right-lateral El Tigre fault (Bastías and Bastías, 1987; Siame et al., 1997; Siame et al., 2006; Cortés et al., 1999b).

South of 31°30′ S, in the Precordillera Sur, geomorphic and structural evidence of Quaternary deformation have been traditionally observed on the active front at the eastern border of the Precordillera (Bastías et al., 1993). Here again new neotectonic evidence were found to the west of the active front near the western border of the Precordillera Sur (Cortés and Cegarra, 2004; Terrizzano et al., 2007). At 32° S, the Barreal-Las Peñas belt seems to concentrate a large part of the Quaternary deformation of the Precordillera Sur (Cortés et al., 2005a; Cortés et al., 2006). There, the western piedmont of the Precordillera has been uplifted during the Quaternary by means of folds, blind faults, faults that shear the surface and faulted blocks that form discrete brittle–ductile shear zones (i.e. Loma de Los Avestruces high) at different scales. At the Barreal-Las Peñas belt, the association of contractional and strike-slip structures, their orientation and the kinematic indicators of faults are consistent with a left-lateral transpressive deformation (Cortés et al., 2005b).

The central region of the Precordillera Sur (32°20′ S) is characterized by NE trending faults scarps with evidence of local extensional deformation (Cortés et al., 1999b). There, the San Bartolo fault displays a complex association of geomorphic, stratigraphical and structural features of Quaternary deformation (Pasini, 1999).

Our studies were carried out in three areas of the Precordillera with significant Quaternary tectonic activity. They are: (i) the San Bartolo fault, in the southern region of the Precordillera Sur (Fig. 2); (ii) the Los Avestruces high, in the western piedmont of the Barreal-Las Peñas belt (northern region of the Precordillera Sur, Fig. 3) and (iii) the El Tigre fault, in the central segment of the Precordillera (Fig. 4).

3. ERT surveys: equipment and methodology

The location of the seven geoelectric profiles (SB1, SB2, A1, T1, T2, T3, T4) is presented in Figs. 2–4. Measurements were performed with a Syscal R1 Plus Switch 48 Georesistivimeter (Iris Company), which can be connected to a linear array of 48 electrode nodes, with a 10 m of maximum spacing. The electrodes are connected on the back of the resistivimeter by means of two strings of heavy-duty seismic-like cable with 24 output each. Acquisition and geometric parameters (maximum permitted standard deviation of the measurement, minimum and maximum numbers of stacks per measurement, input current time per cycle and desired signal voltage) have to be set. The resistivimeter is able to automatically perform the pre-defined sets of measurements according to the type of array selected and provides direct reading of input current, potential difference, electrode location and apparent resistivity. Geometric parameters n (level) and d (electrode spacing) were assigned according to the desired maximum depth of investigation and noise level.

The problem of finding an inverse 2D model of resistivity distribution in a profile was solved numerically in the form of a simple rectangular cell model by means of the RES2DINV program, of Geotomo software (Loke, 2001; Loke, 1996-2002). This program allows to estimate the resistivity of the cells (*model parameters*) that adjusts the quantities measured at surface, within certain discrepancy. At first, the quantities derived from the field measurements are presented in the form of a *pseudosection*, a contour diagram

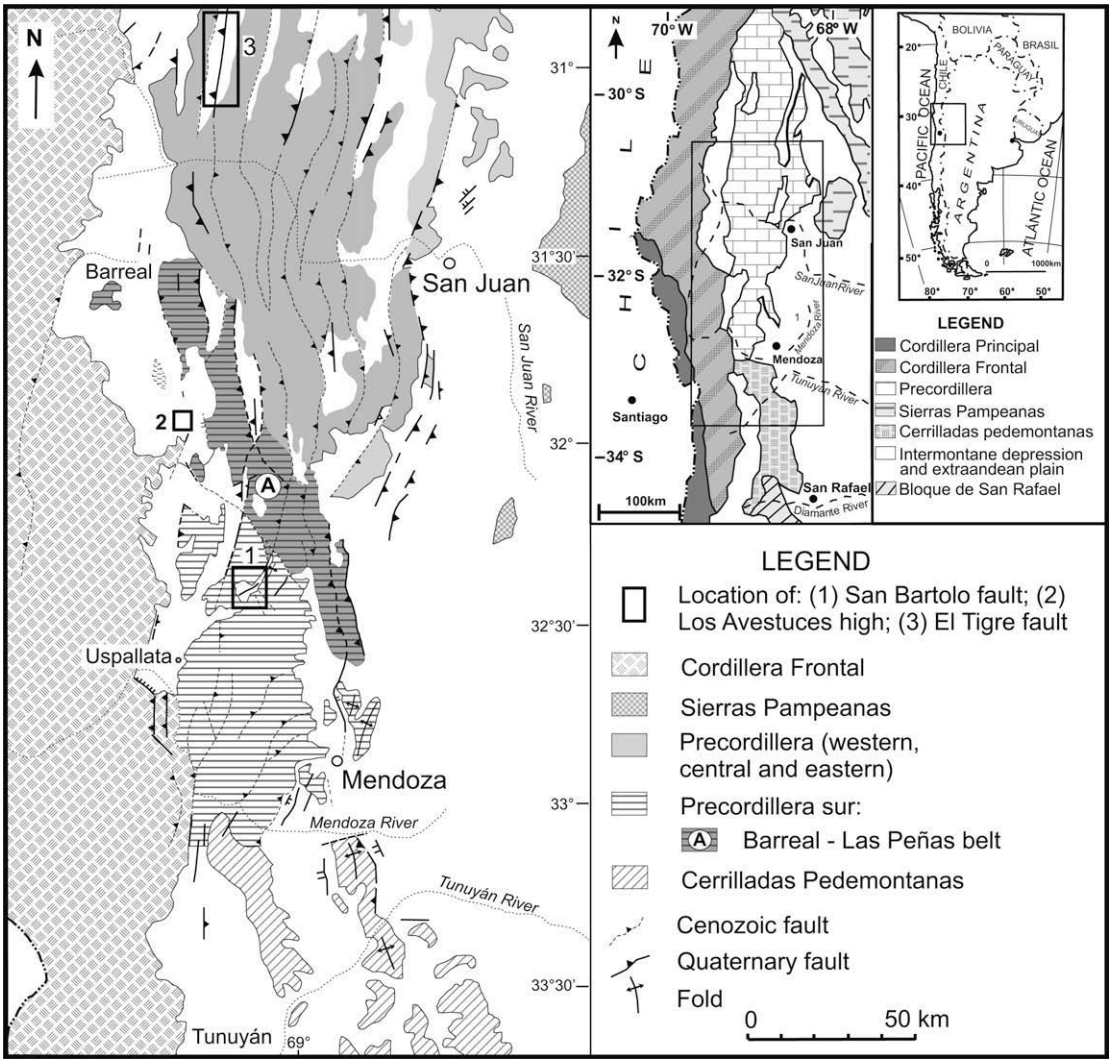

Fig. 1. Map of main Quaternary structures in the Central Andean Precordillera of western Argentina (from Cortés et al. (2005a, 2006)).

in which the *apparent resistivity* values are assigned to a predefined location according to the array type used (Telford et al., 1990). During the inversion routine the initial model parameters are modified and improved by solving a least-squares equation (Lines and Treitel, 1984). This Gauss–Newton equation determines the corresponding change in the model parameters that should reduce the sum of squares of the discrepancies between the apparent resistivity values calculated from the cell model and the apparent resistivity values deduced from the real field data, and also minimizes the change in the model parameters between iterations *(smoothness-constrained least-squares method*). The discrepancy between the calculated values of apparent resistivity and those inferred from field data are expressed through the root mean square (*RMS*). A modification can also be introduced in the optimization algorithm which consists in minimizing the sum of squares of the spatial changes in the model parameters (*smoothness-constrained least-squares method with smoothing of model resistivity*), thus the model resistivity values in the section change in a smooth manner. An alternative optimization method is the *blocky inversion* (Loke et al., 2001), in which the quantity to be reduced is the sum of absolute values of the discrepancies. In this occasion, a final model with sharp boundaries and homogeneous resistivity distribution within the bodies is expected (*robust modelling* alternative). Finally, a contour diagram based in the resistivity distribution of the model constitutes the ERT.

In this work, the forward modelling subroutine (calculus of apparent resistivity from resistivity model parameters) and Jacobian matrix calculation were performed both by finite element method. For the inverse model, the smoothness-constrained least-squares method (reduction of l_2 *norm* or *Euclidean norm*) with smoothing of model resistivity values was generally used, except for one profile (SB2), where blocky inversion gave better results. Topography information in the cell model was incorporated by means of a distorted finite-element mesh: all nodes along the same vertical line are shifted the same amount according to the elevation of the ground surface (*uniformly distorted grid*). The investigation depths depended on the number n of levels chosen, the electrode separation, the total length of profiles and the type of array. The results of the geoelectric tomographies are described and shown in the following section.

4. ERT results and interpretation

4.1. San Bartolo fault

The western margin of the San Bartolo range (Fig. 2) is limited by, approximately, a 2-km-wide fault zone, which is constituted by a main fault scarp associated with "in line" and drag folds and splays that in some cases bound rhomboidal blocks. Fault scarps and blocks were formed in Triassic rocks (the Uspallata Group)

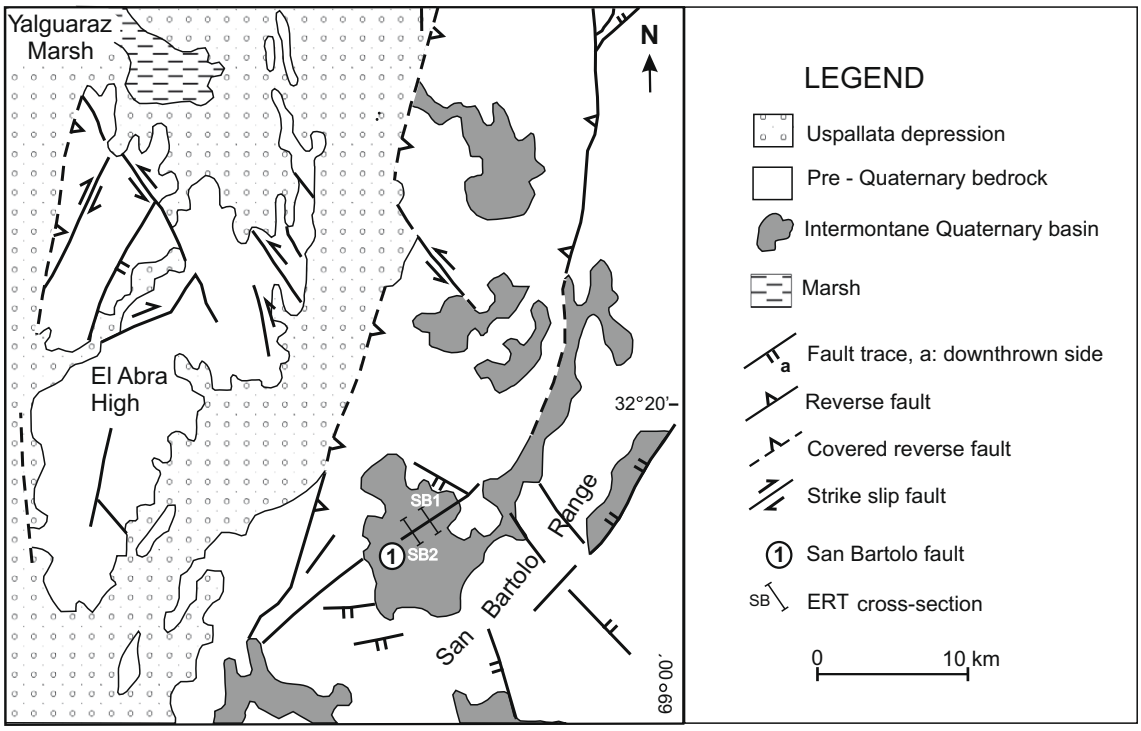

Fig. 2. Map of Cenozoic structures of the central-western Precordillera of Mendoza (from Fazzito et al. (2006)). The two ERT cross sections across the San Bartolo Fault are indicated.

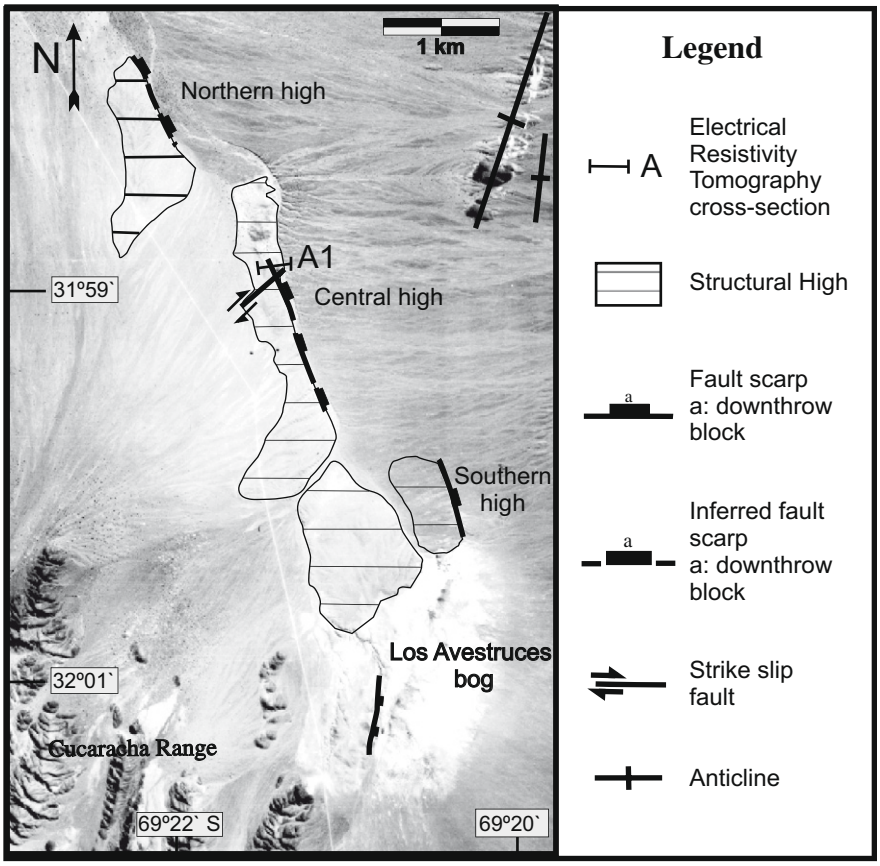

Fig. 3. Partially interpreted aerial photograph of Los Avestruces high. Quaternary structures and A1 ERT cross section are indicated.

as well as in Pleistocene unconformably overlying alluvial deposits (Pájaro Muerto Formation). In this area, the fault is exposed as a north-east trending bedrock scarp that changes into a composite piedmont scarp to the southwest, in the sense of Stewart and Hancock (1990, 1991). Its height decreases from 40 m in the NE to a few meters in its southwestern end. Scarce kinematic information

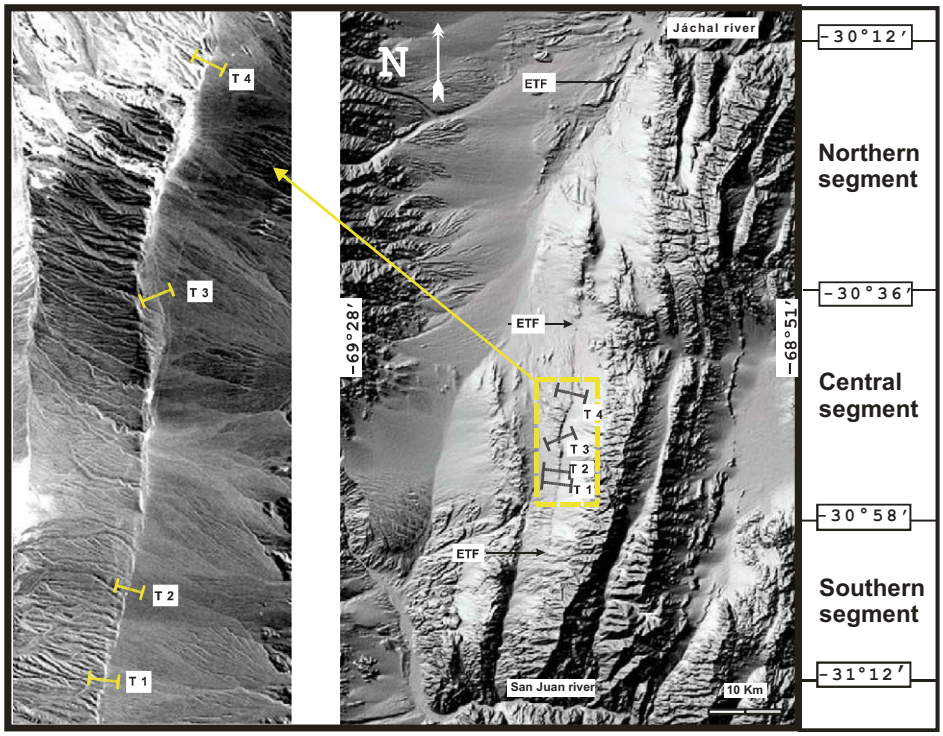

Fig. 4. Satellite image (left) and Digital Elevation Model (right, image from SRTM, 3 arc second, available at http://seamless.usgs.gov) of the El Tigre fault with the approximate location of the four ERT cross-sections (T1, T2, T3 and T4) performed in its central segment.

in minor faults and the orientation of oblique folds and faults at surface show a structural association consistent with a transtensive regime (Pasini, 1999). However it is not possible to verify, by direct observation of the fault plane, whether the relative vertical component of motion is governed by a normal or a reverse fault. In this case, three surveys along two cross-sections of the main fault were carried out to determine the subsurface geometry of the fault plane. This intends to determine the Quaternary tectonic regime of the San Bartolo fault zone (i.e. transpressive or transtensive).

4.1.1. Cross-section SB1 (bedrock scarp)

Two surveys along the same cross-section but with different arrays were performed across this fault scarp, one with a Wenner–Schlumberger (WS) array (see associated inversion in Fig. 5a) and the other with a dipole–dipole (DD) array (Fig. 5b). In both cases a 470 m long survey was recorded with 48 electrodes and a separation of 10 meters, with $n = 1–25$ (n an integer), which produced a total number of 529 and 825 quadripoles for the WS and DD arrays, respectively. Time of current injection was 1 s and a minimum of 3 and maximum of 6 repeated measurements at each point was designed in order to obtain a standard deviation <3% for each apparent resistivity value. The contour of the common surveyed area is marked on Fig. 5a with a dotted line. In the first tomography, with a modelled maximum penetration depth of 83 m, a significant lateral resistivity variation between about 240 m and 340 m at surface is detected, outlining a high conductive zone with resistivity values below 100 Ω m. This feature stands around the localization of the scarp, suggesting that the low resistivity region corresponds to the fault zone in the subsurface. A moderately west dipping fault zone is inferred from the tomographic model. This and the relative displacement observed at the scarp indicate an extensional slip component in the fault, with the hanging wall to the west. Therefore, the ERT permits to characterize the San Bartolo Fault at this locality as a normal fault. A high resistivity (>1000 Ω m) zone imaged in the subsurface model at the upper part of the eastern block (profile length (PL) >330 m) is consistent with outcropping consolidated Triassic clastic rocks. A second low resistivity anomaly at around 220 m ($\rho \approx 150\ \Omega$ m) seen in both ERT is interpreted as an extensional antithetic blind fault associated to the main San Bartolo fault system. The variable distribution of low and high resistivities along the top 30 m of the western block suggests the presence of other normal faults of the same antithetic set (Fig. 5a and 5b).

The DD array was performed with the same electrode separation and position than the WS previously described, and gave a modelled penetration depth of around 50 m. This resistivity model is remarkably coincident with the previous tomography, supporting the interpretation of the previous ERT. Mainly, the San Barolo fault zone is again clearly defined as a west-dipping low resistivity region. The second low resistivity anomaly at PL = 220 m and the variable resistivity pattern on the west block are also present. The DD model, however, shows some differences. In particular, the surficial resistivity distribution on the eastern end of the section shows the high resistivity associated to the Triassic rocks outcropping beyond the 400 m. This is in contrast with the field observation of exposures immediately to the east of the scarp and the WS ERT.

4.1.2. Cross-section SB2 (piedmont scarp)

At approximately 800 m to the south of cross-section SB1, a second ERT with a DD array was recorded across the San Bartolo fault scarp. In this case, the cross-section corresponds to a piedmont scarp with no exposures of consolidated rocks. Surficial observations indicate that the scarp affects Pleistocene unconsolidated alluvial sediments. The DD ERT with 48 electrodes and 470 m length was obtained with two different dipole lengths: $d = 10$ m ($n = 1–10$) and $d = 20$ m ($n = 5–12$). This yielded 621 quadripoles. Same stacking parameters and injection time were used. Similarly to cross-section SB1, the resistivity model of Fig. 6 images a strong

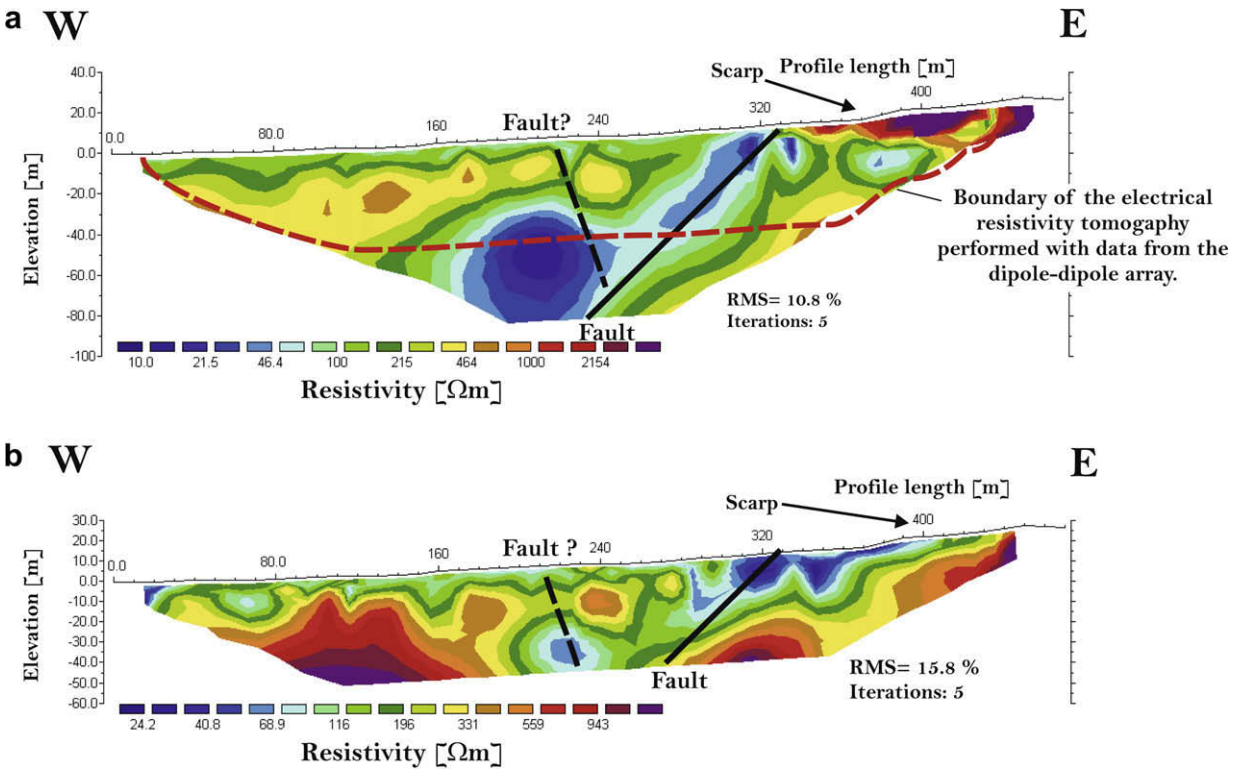

Fig. 5. Electrical resistivity tomographies (ERT) along cross-section SB1 across the San Bartolo bedrock fault scarp. (a) Resistivity model corresponding to WS array with 10 m electrode separation. Its maximum penetration depth was 83 m. (b) Resistivity model corresponding to DD array with electrodes separated 10 m. The depth of the tomography is of 51 m.

surficial lateral resistivity drop between 160 m and 260 m, which defines a conductive region dipping to the west with resistivity values lower than 50 Ω m. This region lies beneath the fault scarp and is interpreted again as the San Bartolo fault zone. In this case, the fact that the scarp was developed in Quaternary unconsolidated sediments is reflected by lower resistivity values than in SB1 at both sides of the scarp (150–900 Ω m). The overall consistency of the ERT indicates that the interpretation of San Bartolo as a west dipping normal fault is a robust one. The characteristic very low resistivity values along the fault zone suggest an increased permeability of this area, and points to a possible diagnostic electrical feature of this fault. However, the wide low resistivity zone limits the resolution on the exact location and geometry of the fault plane, interpreted in Fig. 6, similar to what happened with the previous profiles In this case the low resolution of the fault zone from the resistivity characteristics does not permit any accurate determination of the fault plane dip. A tentative trace has been depicted in Figs. 5 and 6. This uncertainty, however, does not preclude to interpret that the fault zone is likely dipping west and that the latest displacements that produced the scarp correspond to an extensional regime.

4.2. Los Avestruces high

The Los Avestruces high is located in the western piedmont area of the Barreal-Las Peñas belt in the Precordillera Sur, where a strong pattern of paleotectonic anisotropies is present. Its morphotectonic features, in contrast with other zones of the Precordillera, are partially controlled by Late Cenozoic reactivation and tectonic inversion of Permian to Triassic structures (Cortés et al., 2005b; Terrizzano et al., in press). This region of the Precordillera Sur overlaps with the northern branch of the Triassic Cuyana basin (Legarreta et al., 1993; Ramos and Kay, 1991; Cortés et al., 1999a). These Mesozoic structures, then, may have played an important role in the development of the youngest deformation.

The Los Avestruces blocks comprise a set of 1–2 km long structural highs developed on Quaternary alluvial fans in the western margin of the Barreal-Las Peñas belt. Its *en-échelon* morphotectonic arrangement defines a minor NW trending sinistral transpressive zone (see Fig. 3). Recent neotectonic investigations in this region showed clear evidences of Quaternary deformation. At least three faulted and tilted piedmont aggradation levels and alluvial fan deposits have been determined there (Cortés and Cegarra, 2004; Terrizzano, 2006; Yamin, 2007).

The Los Avestruces zone shows fault scarps developed in Pleistocene levels. Outcrops of Quaternary deposits are still preserved as high remnants on top of the structural blocks. The highs are obliquely segmented by NE trending faults. In order to complement the ongoing Neotectonic investigations in the area with information about the subsurface geometry of the structurally controlled geomorphic features, one ERT cross-section was obtained across this structure. This profile crosscuts, from west to east, the westernmost edge of the central structural high in Pleistocene deposits, a NNW fault scarp facing to the east, a small outcrop of Paleozoic clastic metasediments which bounds the central high and Quaternary alluvial deposits of the Precordillera.

4.2.1. Cross-section A1

A 470 m long DD array was used in this site, with 48 electrodes separated by 10 m. Five hundred and forty five quadripoles were determined with dipole length of 10 m (n = 1–6) and 20 m (n = 3–12). A maximum penetration of 60 m was modelled. Injection time was 1 s and 2–6 repeated measurements were performed at each quadripole.

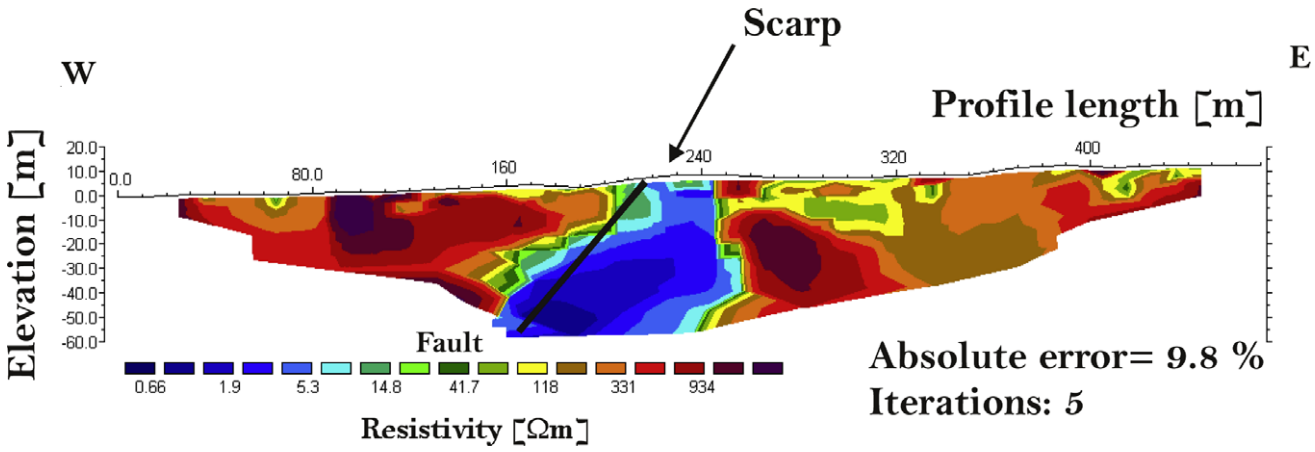

Fig. 6. Electrical Resistivity Tomography (blocky inversion) performed across piedmont scarp in San Bartolo fault corresponding to DD array. Unit electrode spacing was 10 m and the final maximum penetration depth was 59 m.

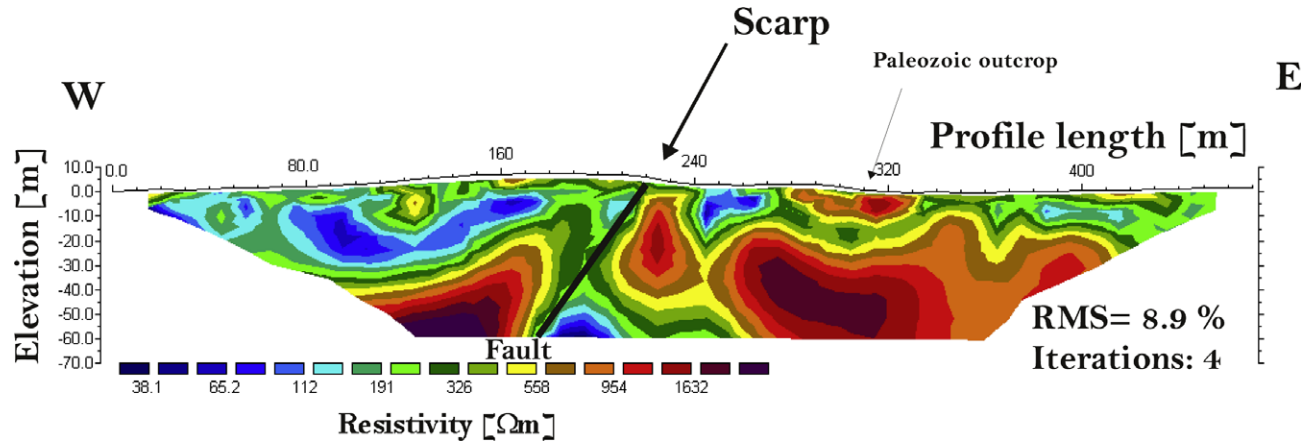

Fig. 7. Electrical Resistivity Tomography performed in the Los Avestruces highs. A DD array was used with a unit electrode spacing of 10 m (smooth-constrained inversion). Maximum penetration depth was 60 m.

Fig. 7 shows the inverse model for the subsurface resistivity at this site. The scarp has a small topographic relief and it is located at distance 220 m, showing an uplifted western block. The inverse model is consistent with the presence of Quaternary alluvial fans beds ($\rho < 325\ \Omega$ m) both at the western (PL < 180 m) and the eastern side (PL > 330 m) of the scarp. Beds on the western side are apparently dipping west, opposing the regional and original slope, which suggests that the Quaternary infill has been affected by tectonic tilting. A conspicuous resistivity discontinuity is evident in the subsurface coincident with the location of the fault scarp. This suggests that the scarp is associated to a west-dipping high-angle fault. Exposures of Paleozoic metaclastic rocks to the east of the scarp (PL = 320 m) which coincide with high resistivity values in the inverse model, allow to assign the high resistivity zones ($\rho > 900\ \Omega$ m) in the subsurface to these rocks A significant throw of around 25 m is therefore estimated from the resistivity distribution across the fault. Since the distribution of the Paleozoic rocks indicates that the hanging western block is down-thrown, the fault acted as a normal fault after the Lower Paleozoic. This is opposite to the reverse movement indicated by the Quaternary sediments displaced along the scarp. The only possible reconciliation to these observations is to interpret the Los Avestruces fault as an ancient extensional fault, probably associated with the Cuyana Basin, that has been reactivated as a contractional fault in the Quaternary (Terrizzano et al., 2006). The extensional throw was larger than the Quaternary contractional displacement allowing us to infer the tectonic inversion. This small scale survey confirms the tectonic pattern of the area characterized by Late Cenozoic reactivation of Late Paleozoic–Early Mesozoic structures.

4.3. The El Tigre fault

The El Tigre Fault (see Fig. 4) is a 120 km-long right-lateral strike-slip fault located in the western region of the central segment of the Precordillera, in the San Juan province, close to the Calingasta-Iglesia Valley (Fig. 1, 29°–31° S; Bastías and Bastías, 1987; Bastías et al., 1990,1993; Siame et al., 1997, 2006). Surface disruptions and geomorphic features like fault scarps, sag ponds, pressure ridges and offset streams constitute the evidence for a significant Quaternary activity of this fault. The Quaternary sediments disrupted by the fault are mainly Middle to Upper Pleistocene alluvial fans. The fault has a mean N10° E strike. Considering the fault trace geometry, Siame et al. (1997) proposed a subdivision into three main segments: south, central and north of 26, 48 and 46 km long, respectively. Siame et al. (2006) have suggested that the El Tigre fault is a major crustal fault accommodating a dextral strike-slip component (1 mm yr^{-1}) due to partitioning of deformation induced by an oblique convergence of the Nazca plate under South America. The geoelectrical survey presented here was carried out in the central segment of the El Tigre fault. This is a complex fault zone, with several releasing and restraining zones, that are the product of bends and splays on the fault trace. A releasing area is

always marked by a sag pond or a small pull-apart basin within the alluvial fans, while a restraining area is marked by a pressure ridge. The presence of an east-facing steep slope, commonly bounded by several sag ponds on its eastern foot and by beheaded streams on its western side were interpreted by Siame et al. (1997, 2006) as a result of an oblique slip (rake 17°) with an uplift of the western block of the fault (0.3 mm/y).

Six ERT were obtained along four cross-sections in the central segment of the El Tigre fault (Fig. 7). Cross-sections 1–4 were located perpendicular to the fault trace and separated of each other by 4.5 km (T2-T1), 12.5 km (T3-T2) and 7 km (T4-T3). A total fault stretch of 24 km was therefore covered in our survey.

4.3.1. Cross-section T1

This is the southernmost cross-section (Fig. 4). It was located near the southern end of the central segment of the El Tigre fault. In this area the fault is expressed as a rectilinear single scarp

Two 470 m long ERT across the El Tigre fault trace were obtained. Data was acquired using a WS and a DD arrangement. In both cases similar recording parameters were used: for the WS array, the electrode spacing was 10 m, injection time 2 s and d = 10 m (n = 1–12), while for the DD array d = 10 m (n = 1–6) and 20 m (n = 3–12). This gave, respectively, a total number of 408 and 545 quadripoles. In general, data acquisition was of high quality. The tomographies performed with DD (Fig. 8a) and WS (Fig. 8b) arrays are remarkably similar. In conformity with the presence of a scarp at surface, both sections display a strong lateral resistivity contrast revealing a fault location at around 220 m. This feature could be interpreted as a near vertical fault in total agreement with the strike slip-fault model of the El Tigre Fault. The western block is composed by high resistivity materials (ρ > 200 Ω m) that change to values below 100 Ω m at the interpreted fault plane. The high angle resistivity contrast shows a high-angle west dipping attitude in the DD ERT (Fig. 8a), which should be more resolutive for lateral changes in electrical parameters than the WS survey. This suggests that the fault plane appears highly dipping to the west, indicating a secondary reverse component of displacement at this site of the El Tigre fault. The eastern side of the fault is characterized by significantly lower resistivity values than the western block (ρ = 100–180 Ω m) indicating different lithology on both sides of the fault trace. The eastern block seems to depict a smooth stratification with a slight tilting towards de east. This is much better depicted by the WS array (Fig. 8b), as should be expected, due to its much higher sensitivity to horizontal structures. In addition, both models show relatively high resistivities near the surface at the eastern end, which is apparently caused by an east-thickening level of recent alluvium. In the eastern block, very low resistivity values (ρ < 50 Ω m) below −40 m suggest the presence of significant ground water content (water table?). This indicates that the fault may be acting as a western barrier to water circulation coming from the El Tigre range in the east.

4.3.2. Cross-section T2

This cross-section was located 4.5 km north from T1. From aerial photographs (Fig. 4) and ground observations, this is characterized as a relay zone, with development of at least two parallel scarps. The easternmost (scarp 2, Fig. 9) is apparently the most active in recent times. At this site a 710 m long ERT was obtained by means of the roll-along system (sequential displacement of one half of the entire array (24 electrodes), to yield an effective number of electrodes equal to 72). In such a way the cross section included both scarps. The DD array was used with injection time set at 1 s, d = 10 m (n = 1–6) and d = 20 m (n = 3–10), with a total number of 852 quadripoles. The inverse model of resistivity distribution depicted in Fig. 9 shows a major discontinuity around 500 m. This point coincides with scarp 2. To the east, very high resistivity

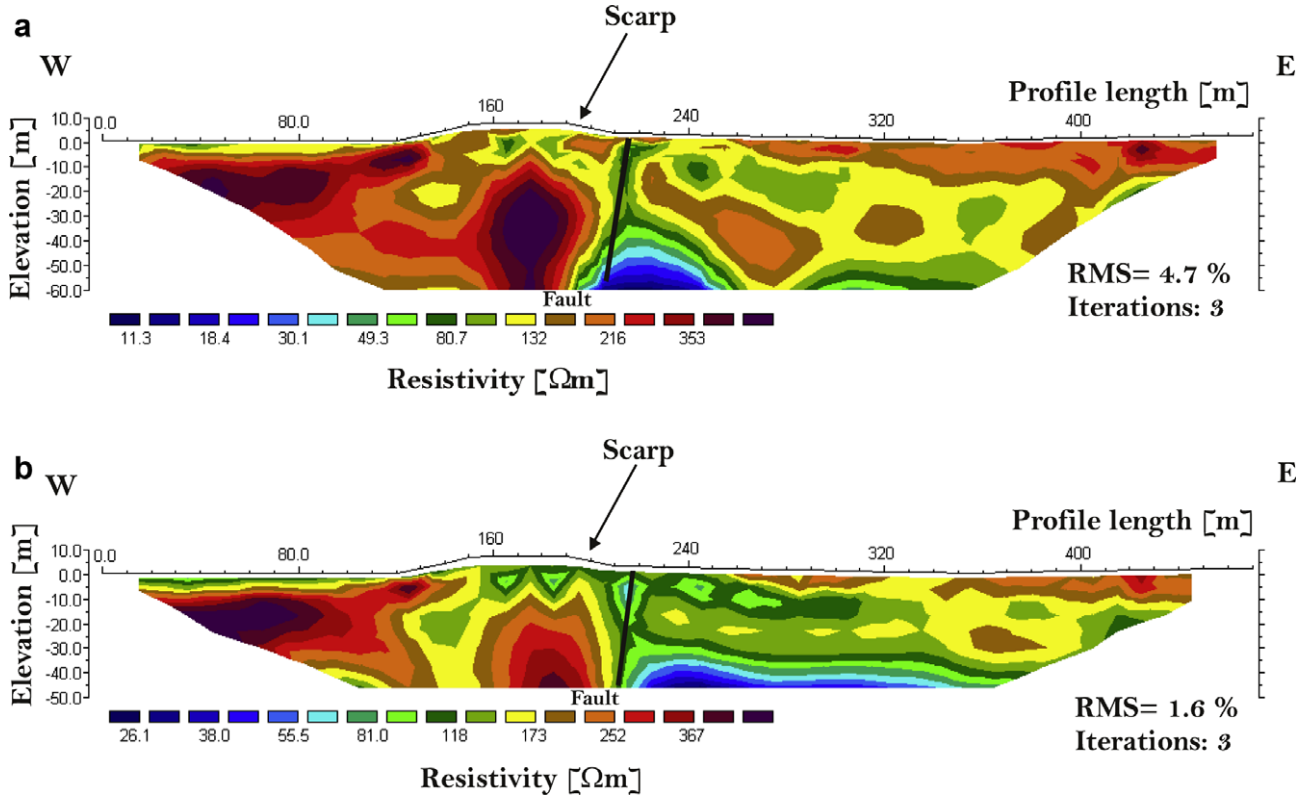

Fig. 8. Electrical resistivity tomographies (smooth inversion) performed across T1 in El Tigre Fault. (a) Resistivity model corresponding to DD array. Unit electrode spacing: 10 m. Maximum penetration depth was 51 m. (b) Resistivity model corresponding to WS array. Unit electrode spacing: 10 m. Maximum penetration depth was 45 m.

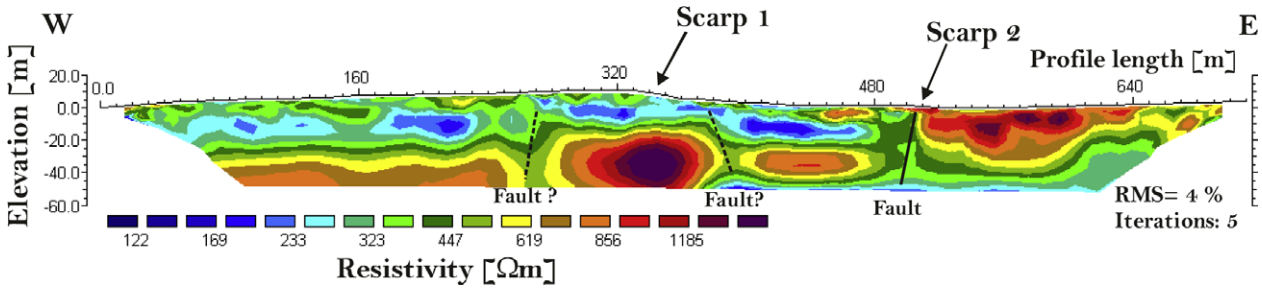

Fig. 9. Resistivity model with smoothness restriction corresponding to El Tigre Fault, across T2 (DD array, roll along method). Unit electrode spacing is 10 m. Maximum penetration depth was 51 m.

values ($\rho > 1000\ \Omega$ m) are typical of the first 30–40 m in depth. A dramatic change is observed to the west with resistivity values under 600 Ω m and the appearance of a subhorizontal conductive layer that extends to the western end of the cross-section at about 20 m below surface. The presence of a near vertical fault is inferred at scarp 2. The width of the low resistivity zone does not permit to discriminate between a vertical or high-angle west dipping fault. This fault has apparently acted as a barrier to ground water as already observed in the previous cross-section. No evidence of discontinuity was found under scarp 1 at 350 m, suggesting that this is not a fault scarp or that this fault did not produce any electrical expression. In addition, two discontinuities suggestive of possible dead or blind splays with no surficial expression are observed at 270 m and 390 m along the deepest 25 m of the section. Further geophysical investigations could solve this uncertainty.

4.3.3. Cross-section T3

This is located 12.5 km north of T2. This area is characterized by a pressure ridge due to a minor bend in the main fault trace. The cross-section comprises at least two scarps, scarp 1 being of likely tectonic origin, while the smaller scarp 2 is of dubious origin. The cross-section however does not cover the whole ridge. A large part of its western part was not surveyed. Two ERT were obtained at this cross-section with a DD array and 48 electrodes. One ERT was performed with the standard 10 m electrode separation (Fig. 10a), while a second one was centred at the same place but obtained with an electrode separation of 5 m. This would allow a higher resolution, both vertical and horizontal, while a smaller penetration. In both cases 503 quadripoles were defined, injection time was 1 s and $d = 10$ m ($n = 1$–6) and $d = 20$ m ($n = 3$–10) for the long one and half the d values for the shorter array. The inversion models of both ERT show a remarkable similarity, indicating that the results are geophysically robust. The overall pattern of resistivity distribution in this case is more complex than the previous examples. Apparently, in this case, the fault zone does not produce a major change of an intermediate depth (15–25 m below surface) conductive level (water table). Lateral changes of resistivity in the lowest 10–20 m of the long cross-section model are apparently suggesting lateral changes in the lithology and may be portraying the presence of one or more fault planes. The most conspicuous plane is depicted at about 190–220 m and corresponds to a west inclined low resistivity zone ($\rho < 100\ \Omega$ m) that bounds a local deep high resistivity zone ($\rho > 400\ \Omega$ m). The eastern margin of the conductive zone corresponds at surface with the scarp. In this case the interpreted fault zone should be a high-angle fault with a reverse component, consistent with the ridges developed in this area. The ERT model obtained from the 5 m electrode separation (Fig. 10b) offers a more detailed image of the shallow subsurface structures. A sharp resistivity contrast is observed at the same location than in the previous model, confirming the likely presence of a fault plane. Its reduced penetration depth, however, is a drawback for clearly identifying the fault planes.

Two subvertical fault planes are speculatively inferred to the east of the previous one at about 250 m and 300 m in the first ERT model (Fig. 10a). They are interpreted as so from the important lateral changes in resistivity values in the deepest part of the model. The inferred fault at 300 m coincides with a second scarp recognized in the field. However, the almost continue low resistivity level at moderate depths (10–30 m) along most of the cross-section partially obscures an unambiguous detection of a fault zone. Therefore, the uncertainty in this cross-section is larger than in the previous ones and the interpretation more tentative. Further ETR in the area or the use of other geophysical methods, like ground penetrating radar (e.g. Demanet et al., 2001) may help confirming or refuting our interpretation.

4.3.4. Cross-section T4

This cross-section was located 7 km north from T3. It corresponds to the southern end of a released area that have produced a small pull-apart basin. The cross-section was performed along a creek that dissects the main fault scarp. An ERT with a 470 m DD array was performed here. The acquisition parameters used were: time injection, 1 s; $d = 10$ m ($n = 1$–6) and $d = 20$ m ($n = 3$–12); so 545 quadripoles were predefined. This ERT shows (Fig. 11) a significant different pattern of resistivities on both sides of the scarp, with much higher resistivities to the east, opposite to the resistivity distribution observed in T1. Since T4 was recorded along a small creek dissecting the scarp, no topographic evidence of the scarp can be seen along the model. The inferred location of the scarp was obtained from interpolation of its trace (from observations both north and south of the cross-section). To the east, a very well defined inverse stratification of the resistivity is observed. This resembles the pattern also observed at T1 (Fig. 8b). This pattern corresponds to stratified alluvial sediments and the decrease in resistivity at depth is likely related to an increase in water content of the sediments. A significant fall in resistivity values can be observed between 100 m and 140 m. In the subsurface, this is seen as an irregular area of very low values ($\rho < 20\ \Omega$ m). The disappearance of the eastern pattern and the presence of a near vertical low in resistivity at the position of the scarp is a clear indication that these features are related to the presence of the fault zone at depth. Sediments exposed on the western side correspond to high porosity Late Pliocene–Pleistocene (?) unconsolidated sands and silts with likely high fluids content as suggested by the ERT. Although the geometry of the fault zone is not precisely imaged by the electrical properties in this case, a near vertical fault is consistent with the geological background and the ERT model. A second, blind fault, has been speculatively interpreted from the geophysical results, 20–30 m to the east. A sharp lateral decrease in resistivity values at around 165 m from −10 m to −40 m at depth, which seems not to affect the most surficial layer of high resistivity, suggests the presence of an associated secondary fault that did not affect the most recent deposits, which explains why it cannot be determined geomorphically.

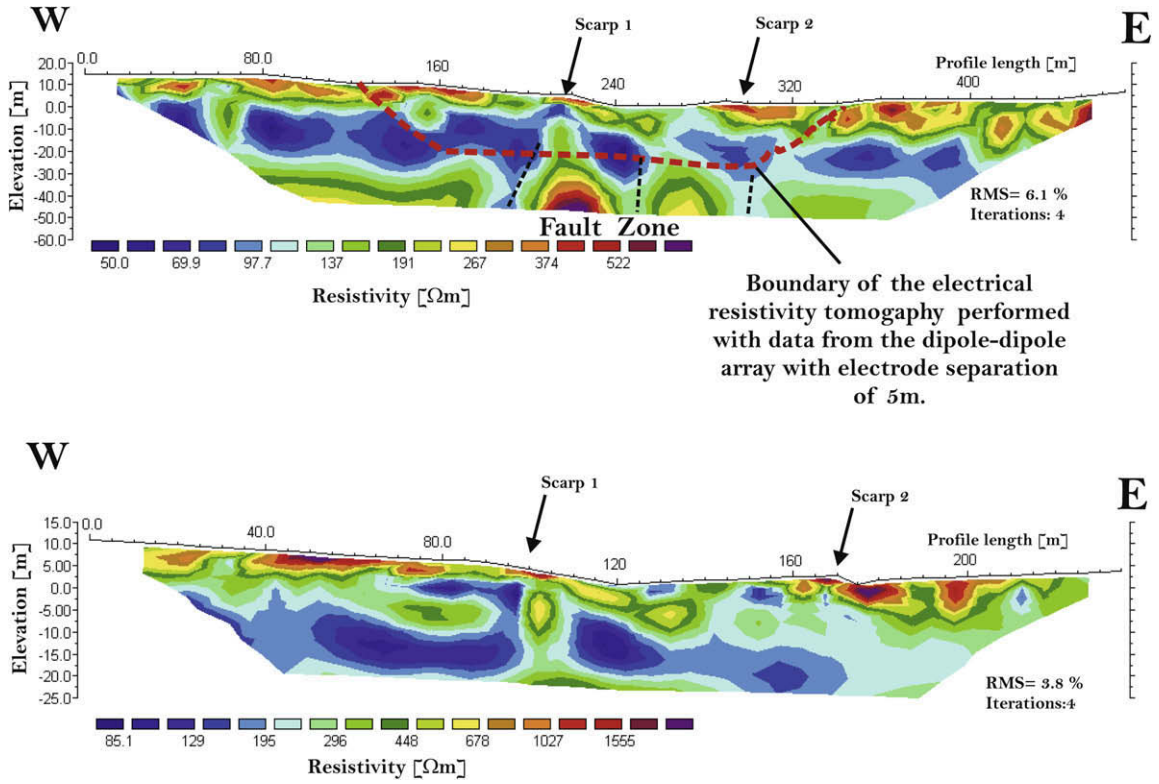

Fig. 10. Electrical resistivity tomographies (smooth inversion) performed across T3. (a) Resistivity model corresponding to DD array. Maximum penetration depth was 50 m. (b) Resistivity model corresponding to DD array with unit electrode spacing of 5 m. Maximum penetration depth was 25 m.

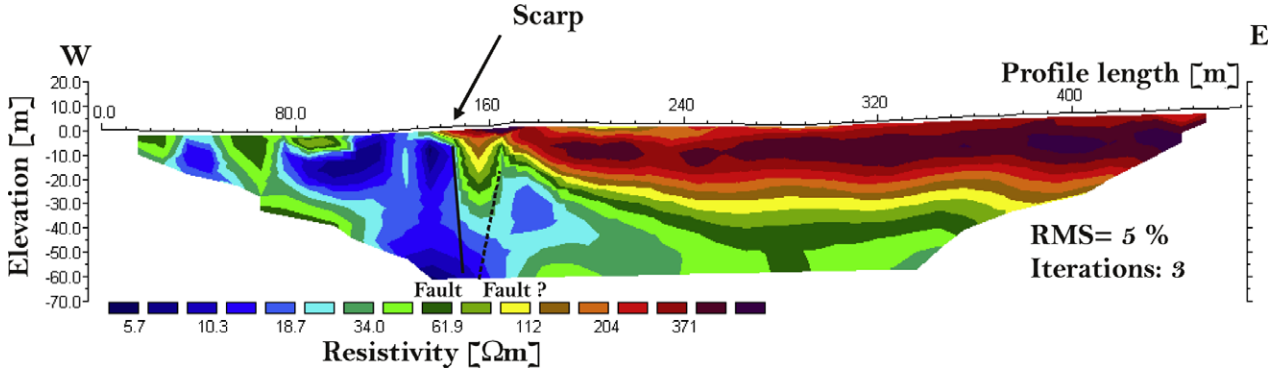

Fig. 11. Resistivity model (smooth inversion) carried out across El Tigre Fault, DD array. Unit electrode spacing was 10 m. Maximum penetration depth was 61 m.

5. Discussion and conclusions

Electrical resistivity tomographies across three different fault zones in the Precordillera of western Argentina were reported, providing useful information regarding the Neotectonic activity in the region. This methodology was applied where all previous research has been only of geological and geomorphical nature.

Studies were performed across: (i) the apparently transtensive San Bartolo fault, in the Precordillera Sur; (ii) the Los Avestruces transpressive high, near the northwestern border of the Precordillera Sur and (iii) the strike-slip El Tigre fault zone in the Western Precordillera.

The subsurface fault plane orientation obtained from ERT images combined with geomorphological data allowed us to characterize San Bartolo at the study locality as an extensional fault.

A significant control of the pre-Cenozoic structures on the neotectonic deformation at the Los Avestruces highs in the Barreal del Leoncito area (Uspallata-Calingasta Valley) were confirmed by the ERT method. This showed an ancient extensional fault, probably associated with the development of a Triassic Basin, that has been reactivated as a contractional fault in the Quaternary.

Electrical images across the El Tigre fault (Western Precordillera) are consistent with previous geomorphical information supporting near vertical to high-angle fault planes of a dominantly strike-slip fault. Four ERT cross sections on the El Tigre fault showed a complex and variable interplay between structural, lithological and hydrological features across the fault zone.

The presence of blind or dead splays associated to the main fault in both the San Bartolo and El Tigre were suggested by the ERT inverse models of these fault zones.

On general grounds, our results demonstrate that the ERT method is an economic, speedy and reliable tool to be applied in areas of Quaternary and active tectonics.

Our studies confirm previous results that have demonstrated that resistivity modelling is an effective geophysical method (Fleta et al., 2000; Giano et al., 2000; Storz et al., 2000; Suzuki et al., 2000; Verbeeck et al., 2000; Demanet et al., 2001a, 2001b; Caputo et al., 2003, 2007; Wise et al., 2003; Colella et al., 2004; Rizzo et al., 2004; Nguyen et al., 2005, 2007) to locate, image and characterized Quaternary active faults. In our examples, the ERT method proved to be a successful tool to locate, and in cases to determine the orientation, of the fault planes at subsurface. In several cases the fault zone itself was recorded as a zone with a significantly lower resistivity. Although generally the anomalous zone was too wide to permit a precise definition of the location of the plane and its inclination, its general position and orientation could be inferred. Fault planes were also identified as narrow zones with a remarkably high resistivity contrast at subsurface. The distribution of electrical resistivity on both sides of these structures permitted to infer areas where the fault plane acted as a hidrogeological barrier.

Although in our case the dipole–dipole array was generally used, when a Wenner–Schlumberger array was applied similar results were obtained.

Considering that ERT is a relatively fast and economic geophysical method its systematic application in areas of neotectonic activity may be a cost-effective tool to better characterize the tectonic deformation and to help in active fault hazard assessments. It could also be used as a preliminary method to image the subsurface up to around 100 m deep in advance of other geophysical methods (like shallow reflection seismology) and/or trench excavation.

Acknowledgements

The authors would like to thank the Universidad de Buenos Aires and CONICET for institutional support in this research. Financial support was provided by grants UBACyT X221, UBACyT X262 and PIP-CONICET 5422 projects. Joaquín Rossello kindly collaborated during the field work. We are very grateful to Franck Audemard and an anonymous reviewer for the comments and corrections that improved the paper.

References

Baldis, B.A., Beresi, M.S., Bordonaro, L.O., Vaca, A., 1982. Síntesis evolutiva de la Precordillera Argentina. In: 5° Congreso Latinoamericano de Geología, Actas IV, Buenos Aires, 399–445.

Bastías, H.E., Bastías, J.A., 1987. Análisis de desplazamientos y velocidades en el área diferencial Precordillera, provincia de San Juan. Revista de la Asociación Geológica Argentina XLII (3-4), 261–266.

Bastías, H., Uliarte, E., Paredes, J.D., Sanchez, A., Bastías, J., Ruzycki, L., Perucca, L., 1990. Neotectónica de la provincia de San Juan. In: 11° Congreso Geológico Argentino, Relatorio, San Juan, 228–244.

Bastías, H., Tello, G.E., Perucca, L.P., Paredes, J.D., 1993. Peligro sísmico y neotectónica. In: Ramos, V.A. (Ed.), Geología y Recursos Naturales de Mendoza XII, Congreso Geológico Argentino y II Congreso de Exploración de Hidrocarburos (Mendoza), Relatorio, VI-1, pp. 645–658.

Caputo, R., Piscitelli, S., Oliveto, A., Rizzo, E., Lapenna, V., 2003. The use of electrical resistivity tomographis in active tectonics: examples from Tyrnavos Basin, Greece. Journal of Geodynamics 36, 19–35.

Caputo, R., Salviulo, L., Piscitelli, S., Loperte, A., 2007. Late Quaternary activity along the Scorciabuoi fault (Southern Italy) as inferred from electrical resistivity tomographies. Annals of Geophysics 50 (2), 213–223.

Colella, A., Lapenna, V., Rizzo, E., 2004. High-resolution imaging of the high agri valley basin (Southern Italy) with electrical resistivity tomography. Tectonophysics 386, 29–40.

Cortés, J.M., Cegarra, M., 2004. Plegamiento cuaternario transpresivo en el piedemonte suroccidental de la Precordillera sanjuanina. Asociación Geológica Argentina, Serie D, Publicación Especial No. 7: 68-75, Buenos Aires.

Cortés, J.M., Costa, C.H., 1996. Tectónica Cuaternaria en la desembocadura del Río Las Peñas, borde oriental de la Precordillera de Mendoza. In: 13° Congreso Geológico Argentino y 3° Congreso de Exploración de Hidrocarburos (Buenos Aires), Actas 2, 225–238.

Cortés, J.M., Gonzalez Bonorino, G., Koukharsky, M.L., Brodkorb, A., Pereyra, F., 1999a. Hoja geológica 3369-09, Uspallata, provincia de Mendoza. Servicio Geológico Minero Argentino Boletín, 281 (Buenos Aires).

Cortés, J.M., Vinciguerra, P., Yamín, M., Pasini, M.M., 1999b. Tectónica Cuaternaria de la Región Andina del Nuevo Cuyo (28°–38° LS). In: Caminos, R. (Ed.), Geología Argentina. Subsecretaría de Minería de la Nación, Servicio Geológico Minero Argentino, Anales 29, Cap. 24, 760–778, Buenos Aires.

Cortés, J.M., Pasini, M.M., Yamin, G., 2005a. Paleotectonic controls on the distribution of quaternary deformation in Southtern Precordillera, Central Andes (31° 30′–33° SL). In: International Symposium on Andean Geodynamics, Extended Abstracts: 186–189, Barcelona.

Cortés, J.M., Yamín, M.G., Pasini, M.M., 2005b. La Precordillera Sur, Provincias de Mendoza y San Juan. 16° Congreso Geológico Argentino, La Plata, Actas 1, pp. 395–402.

Cortés, J.M., Casa, A., Pasini, M.M., Yamin, M.G., Terrizzano, C.M., 2006. Fajas oblicuas de deformación neotectónica en Precordillera y Cordillera Frontal (31°30′–33°30′ LS). Controles paleotectónicos. Revista de la Asociación Geológica Argentina 61 (4), 639–646 (Buenos Aires).

Costa, C.H., Rockwell, T., Paredes, J., Gardini, C., 1999. Quaternary deformations and seismic hazard at the Andean orogenic front perspective. In: 4° International Symposium on Andean Geodynamics, Proceedings, pp. 187–191.

Costa, C.H., Gardini, C., Diederix, H., Cortés, J., 2000a. The Andean orogenic front at Sierra de Las Peñas-Las Higueras, Mendoza, Argentina. Journal of South American Earth Sciences 13, 287–292.

Costa, C., Machette, M.N., Dart, R.L., Bastías, E., Paredes, N.D., Perucca, L.P., Tello, G.E., Haller, K.M, 2000b. Map and database of quaternary faults and folds in Argentina. United States Geological Survey Open-File Reports 00-108, 75p.

Costa, C.H., Audemard, M.F.A., Bezerra, F.H.R., Lavenu, A., Machette, M.N., París, G., 2006. An overview of the main quaternary deformation of South America. Revista de la Asociación Geológica Argentina 61 (4), 461–479 (Buenos Aires).

Demanet, D., Pirard, E., Renardy, F., Jongmans, D., 2001a. Application and processing of geophysical images for mapping faults. Computers and Geosciences 27, 1031–1037.

Demanet, D., Renardy, F., Vanneste, K., Jongmas, D., Camelbeek, T., Meghraoui, M., 2001b. The use of geophysical prospecting for imaging active faults in the Roer Graben, Belgium. Geophysics 66 (1), 78–89.

Donne, D.D., Piccardi, L., Odum, J.K., Stephenson, W.J., Williams, R.A., 2007. High-resolution shallow reflection seismic image and surface evidence of the upper Tiber Basin active faults (Northern Apennines, Italy). Bollettino della Società Geologica Italiana 126 (3), 326–331.

Fazzito, S., Rapalini, A., Cortés, J.M., 2006. Tomografía geoeléctrica en zonas de fallas cuaternarias: dos ejemplos en la Precordillera centro-occidental de Mendoza, vol. 9. Revista de la Asociación Geológica Argentina, Serie D, Publicación Especial, pp. 41–47.

Fleta, J., Santanach, P., Martinez, P., Goula, X., Grellet, B., Masana, E., 2000. Geologic, geomorphologic and geophysic approaches for the paleoseismological analysis of the Amer fault (NE Spain). In: Workshop Proceedings of HAN2000: Evaluation of the Potential for Large Earthquakes in Regions of Present Day Low Seismic Activity in Europe, Han-sur-Lesse, Belgium, pp. 63–66.

Giano, S.I., Lapenna, V., Piscitelli, S., Schiattarella, M., 2000. Electrical imaging and self-potencial surveys to study the geological setting of the quaternary slope deposits in the Agri high valley (Southern Italy). Annali di Geofisica 43 (2), 409–419.

Isacks, B., Barazangi, M., 1977. Geometry of Benioff zones: lateral segmentation and downwards bending of the subducted lithosphere. In: Talwani, M., Pitman, W. (Eds.), Island Arcs, Deep Sea Trenches and Back Arc Basins American Geophysical Union, Ewing Series, vol. 1, pp. 99–114.

Jordan, T.E., Isacks, B.L., Allmendinger, R.W., Brewer, J.A., Ramos, V.A., Ando, C.J., 1983. Andean tectonics related to geometry of subducted Nazca plate. Geological Society of America Bulletin 94 (3), 341–361.

Kozlowski, E., Manceda, R., Ramos, V.A., 1993. Estructura. In: Ramos, V.A. (Ed.), Geología y Recursos Naturales de Mendoza XII, Congreso Geológico Argentino y II Congreso de Exploración de Hidrocarburos (Mendoza), vol. 18. Relatorio I, pp. 235–256.

Legarreta, L., Kokogian, D.A., Dellapé, D.A., 1993. Estructuración terciaria de la Cuenca Cuyana: ¢cuánto de inversión tectónica? Revista de la Asociación Geológica Argentina 47(1), 1992, 83–86 (Buenos Aires).

Lines, L.R., Treitel, S., 1984. A view of least-squares inversion and its application to geophysical problems. Geophysical Prospecting 32, 159–186.

Loke, M.H., 1996–2002. Tutorial: 2-D and 3-D electrical imaging surveys. Geotomo Software.

Loke, M.H., 2001. Rapid 2-D resistivity and IP inversion using the least-squares method. Geoelectrical Imaging 2-D and 3-D. Geotomo Software.

Loke, M.H., Acworth, I., Dahlin, T., 2001. A comparison of smooth and blocky inversion methods in 2-D electrical imaging surveys. In: ASEG 15th Geophysical Conference and Exhibition.

Nguyen, F., Garambois, S., Jongmans, D., Pirard, E., Loke, M.H., 2005. Image processing of 2D resistivity data for imaging faults. Journal of Applied Geophysics 57 (4), 260–277.

Nguyen, F., Garambois, S., Chardon, D., Hermitte, D., Bellier, O., Jongmans, D., 2007. Subsurface electrical imaging of anisotropic formations affected by a slow active reverse fault, Provence, France. Journal of Applied Geophysics 62 (4), 338–353.

Pasini, M.M., 1999. Neotectónica del piedemonte noroccidental del cordón San Bartolo, Precordillera de Mendoza. Trabajo Final de Licenciatura. Universidad de

Buenos Aires, Departamento de Ciencias Geológicas, Buenos Aires, 84p., unpublished.
Ramos, V.A., Kay, S.M., 1991. Triassic rifting and associated basalts in the Cuyo basin, Central Argentina. In: Harmon, R.S., Rapela, C.W. (Eds.), Andean Magmatism and its Tectonic Setting Geological Society of America, Special Paper, vol. 265, pp. 79–91.
Rizzo, E., Colella, A., Lapenna, V., Piscitelli, S., 2004. High-resolution images of the fault-controlled high agri valley basin (Southern Italy) with deep and shallow electrical resistivity tomographies. Physics and Chemistry of the Earth 29, 321–327.
Siame, L.L., Sébrier, M., Bellier, O., Bourlès, D.L., Castano, J.C., Araujo, M., 1997. Geometry, segmentation and displacement rates of the El Tigre Fault, San Juan Province (Argentina) from SPOT image analysis and ^{10}Be datings. Annales Tectonicae 1–2, 3–26.
Siame, L.L., Bellier, O., Sebrier, M., 2006. Active tectonics in the Argentine Precordillera and western Sierras Pampeanas. Revista de la Asociación Geológica Argentina 61 (4), 604–619.
Stewart, I.S., Hancock, P.L., 1990. What is a fault scarp? Episodes 13 (4), 256–263.
Stewart, I.S., Hancock, P.L., 1991. Scales of structural heterogeneity within neotectonic fault zones in the Aegean region. Journal of Structural Geology 13, 191–204.
Storz, H., Storz, W., Jacobs, F., 2000. Electrical resistivity tomography to investigate geological structures of the earth's upper crust. Geophysical Prospecting 48, 455–471.
Suzuki, K., Toda, S., Kusunoki, K., Fujimitsu, Y., Mogi, T., Jomori, A., 2000. Case studies of electrical and electromagnetic methods applied to mapping active faults beneath the thick quaternary. Engineering Geology 56, 29–45.
Telford, W.M., Geldart, L.P., Sheriff, R.E., 1990. Applied Geophysics, second ed. Cambridge University Press, Cambridge, UK. 790p.
Terrizzano, C.M., 2006. Deformación cuaternaria en las Lomitas Negras, cinturón Barreal-Las Peñas, provincia de San Juan. Resúmenes de la XIII Reunión de Tectónica, 57, San Luis, Argentina.
Terrizzano, C.M., Fazzito, S.Y., Cortés, J.M., Rapalini, A.E., 2006. Deformación tardío cenozoica en la zona de la ciénaga de los Avestruces, provincia de San Juan. Resúmenes de la XIII Reunión de Tectónica, 58, San Luis, Argentina.
Terrizzano, C.M., Fazzito, S.Y., Cortés, J.M., Rapalini, A.E., 2007. Quaternary transpressive zones in the Precordillera Sur, Argentina: a structural and geophysical approach. 20. Lateinamerika-Kolloquium, Abstract: 60, Kiel, Alemania.
Terrizzano, C.M., Cortés, J.M., Fazzito, S.Y., Rapalini, A.E., in press. Neotectonic transpressive zones in Precordillera Sur: a structural and geophysical approach. Journal Neues Jahrbuch für Geologie und Paläontologie.
Verbeeck, K., Beatse, H., Vanneste, K., Renardy, F., Van Der Meer, H., Roy-Chowdhury, K., Camelbeeck, T., 2000. Geomorphic and geophysical reconnaissance of the Reppel and Bocholt faults, NE Belgium. In: Workshop Proceedings of HAN2000: Evaluation of the Potential for Large Earthquakes in Regions of Present Day Low Seismic Activity in Europe, Han-sur-Lesse, Belgium, pp. 167–170.
von Gosen, W., 1992. Structural evolution of the Argentine Precordillera: the Rio San Juan section. Journal of Structural Geology 14, 643–667.
von Gosen, W., 1995. Polyphase structural evolution of the southwestern Argentine Precordillera. Journal of South American Earth Sciences 8 (3–4), 377–404 (Great Britain).
Wang, Ch.Y., 2002. Detection of a recent earthquake fault by the shallow reflection seismic method. Geophysics 67 (5), 1465–1473.
Wise, D.J., Cassidy, J., Locke, C.A., 2003. Geophysical imaging of the quaternary Wairoa North Fault, New Zealand: a case study. Journal of Applied Geophysics 53, 1–16.
Yamin, M.G., 2007. Neotectónica del bloque Barreal, margen noroccidental de la Precordillera Sur. PhD Thesis, Universidad de Buenos Aires, Departamento de Ciencias Geológicas, Buenos Aires, 281p, unpublished.
Zapata, T.R., Allmendinger, R.W., 1996. Thrust-front zone of the Precordillera, Argentina: a thick-skinned triangle zone. American Association of Petroleum Geologist Bulletin 80, 359–381.